Thermal Stability of Lithium Nickel Oxide Derivatives. Part II: $Li_xNi_{0.70}Co_{0.15}Al_{0.15}O_2$ and $Li_xNi_{0.90}Mn_{0.10}O_2$ ($x = 0.50$ and 0.30). Comparison with $Li_xNi_{1.02}O_2$ and $Li_xNi_{0.89}Al_{0.16}O_2$

M. Guilmard, L. Croguennec,* and C. Delmas

Institut de Chimie de la Matière Condensée de Bordeaux CNRS and Ecole Nationale Supérieure de Chimie et Physique de Bordeaux, Université Bordeaux I, 87, Av. Dr A. Schweitzer, 33608 Pessac Cedex (France)

Received May 2, 2003. Revised Manuscript Received September 4, 2003

The thermal degradation mechanism of $Li_xNi_{0.70}Co_{0.15}Al_{0.15}O_2$ and $Li_xNi_{0.90}Mn_{0.10}O_2$ ($x = 0.50$ and 0.30) was studied by thermal gravimetric analysis coupled with mass spectrometry. Correlation with in situ X-ray diffraction experiments was then achieved to determine the degradation mechanism and to explain the differences in thermal stability observed depending on the material composition. The degradation occurs in two steps: a first transition between the lamellar phase and a spinel-type phase, and then a second transition between the pseudo-spinel phase and a NiO-type phase through a highly disordered $R\bar{3}m$ phase. Comparison of the thermal stability of the four materials shows that the addition of cobalt in the aluminum partial substituted materials improves the stability, particularly during the first step. The manganese partial substitution for nickel appears to improve the stability of the pseudo-spinel-type phase in comparison with Li_xNiO_2 phases. The general thermal behavior of these deintercalated materials is discussed from the solid-state chemistry point of view.

Introduction

In the scope of general studies on the behavior of lithium nickel oxide derivatives which can be used as a positive electrode material in lithium batteries, we are trying to understand the mechanism involved upon the thermal degradation of the electrode.

In the previous companion paper,[1] the comparison of the thermal degradation mechanism of $Li_xNi_{1.02}O_2$ and $Li_xNi_{0.89}Al_{0.16}O_2$ ($x = 0.50$ and 0.30) was studied by in situ X-ray diffraction correlated with thermal gravimetric analysis coupled with mass spectrometry (TGA/MS). The degradation mechanism was shown to be the same for both types of materials and consists of two steps: the first, corresponding to the lamellar to pseudo-spinel transformation, is accompanied by an oxygen loss only for compounds with an initial (Li + M)/O ratio (M = Ni, Al) smaller than $^3/_4$; the second step corresponds to the progressive transformation to a NiO-type structure through a highly disordered $R\bar{3}m$ phase, with an oxygen loss whatever the initial lithium composition. The two steps occur at different temperatures, depending on the material and the lithium composition. Indeed, according to in situ XRD study, the pseudo-spinel phase appears at 200 °C for $Li_{0.50}Ni_{1.02}O_2$ vs 240 °C for $Li_{0.50}Ni_{0.89}Al_{0.16}O_2$ and at 180 °C for $Li_{0.30}Ni_{1.02}O_2$ vs 200 °C for $Li_{0.30}Ni_{0.89}Al_{0.16}O_2$. Moreover, for the same amount of lithium in the structure, the stability of the pseudo-spinel phase appears larger for aluminum-substituted compounds. The thermal stabilization obtained by partial aluminum substitution for nickel was related to the stability of the Al^{3+} ions in the tetrahedral site, which disturbs the cationic migrations required by the phase transformations observed upon increasing temperature to occur.

Despite the positive effect of partial aluminum substitution for the thermal stability, cycling tests have also shown a decrease of the electrochemical performances of the batteries, in particular with a decrease of the reversible capacity and an increase of the polarization, due to the introduction of electro-inactive cations.[2] Therefore, the partial cobalt substitution for nickel in the $LiNi_{1-y}Al_yO_2$ system was considered as a good means to try to combine both positive effects, i.e. an increasing lamellar character for the structure associated with increasing electrochemical performances induced by Co and an increasing thermal stability induced by Al.[2,3−15] In a recent paper we have reported the synthesis and the electrochemical characterization of

* Corresponding author. Phone: (+33) 5-4000-2234. Fax: (+33) 5-4000-6698. E-mail: crog@icmcb.u-bordeaux.fr.

(1) Guilmard, M.; Croguennec, L.; Denux, D.; Delmas, C. *Chem. Mater.* **2003**, *15*, 4476−4483.
(2) Guilmard, M.; Rougier, A.; Grüne, M.; Croguennec, L.; Delmas, C. *J. Power Sources* **2002**, *115*, 305.
(3) Delmas, C.; Saadoune, I. *Solid State Ionics* **1992**, *53−56*, 370.
(4) Delmas, C.; Saadoune, I.; Rougier, A. *J. Power Sources* **1993**, *43−44*, 595.
(5) Zhecheva, E.; Stoyanova, R. *Solid State Ionics* **1993**, *66*, 143.
(6) Ueda, A.; Ohzuku, T. *J. Electrochem. Soc.* **1994**, *141*, 2010.
(7) Rougier, A.; Saadoune, I.; Gravereau, P.; Willmann, P.; Delmas, C. *Solid State Ionics* **1996**, *90*, 83.
(8) Wang, G. X.; Horvat, J.; Bradhurst, D. H.; Liu, H. K.; Dou, S. X. *J. Power Sources* **2000**, *85*, 279.
(9) Ohzuku, T.; Ueda, A.; Kouguchi, M. *J. Electrochem. Soc.* **1995**, *142*, 4033.

10.1021/cm030340u CCC: $25.00
Published on Web 10/22/2003

the $LiNi_{0.70}Co_{0.15}Al_{0.15}O_2$ phase.[11] The Rietveld analysis of the X-ray and neutron diffraction data of $LiNi_{0.70}Co_{0.15}Al_{0.15}O_2$ synthesized by a coprecipitation method, has shown that a quasi-ideal lamellar structure was obtained for this phase, with less than 1% extra-nickel ions in the interslab space. Nevertheless, note that a segregation tendency for cobalt and aluminum ions was also observed. Cycling tests have shown a very good cycling stability with a high reversible capacity of about 150 mAh/g in the 3−4.15 V range at the C/20 rate.

According to recent publications, the $LiNi_{1-y}Mn_yO_2$ system appears to be very promising in term of thermal stability.[16−18] A high reversible capacity in the 150−200 mAh/g range was also observed by Ohzuku for 50% manganese.[19,20] Nevertheless, the structural and electrochemical characterization of $LiNi_{0.90}Mn_{0.10}O_2$ performed in our laboratory[21] has pointed out the difficulties of obtaining a well-lamellar structure; indeed, about 5% extra-nickel ions was found to be present in the interslab space. Moreover, a decrease of the electrochemical performances with a much lower reversible capacity (∼110 mAh/g) than for $LiNiO_2$ was observed.

In this paper, the thermal degradation mechanisms of $Li_xNi_{0.70}Co_{0.15}Al_{0.15}O_2$ and $Li_xNi_{0.90}Mn_{0.10}O_2$ ($x = 0.50$ and 0.30) are described in detail by using in situ XRD and TGA/MS. A comparison of their thermal behavior with that of $Li_xNi_{0.89}Al_{0.16}O_2$ and $Li_xNi_{1.02}O_2$ ($x = 0.50$ and 0.30) is done to determine the effects of partial cobalt/aluminum and manganese substitutions for the thermal stabilization.

Experimental Section

The $Li_xNi_{0.70}Co_{0.15}Al_{0.15}O_2$ and $Li_xNi_{0.90}Mn_{0.10}O_2$ ($x = 0.50$ and 0.30) phases were obtained by electrochemical lithium deintercalation from $LiNi_{0.70}Co_{0.15}Al_{0.15}O_2$ and $LiNi_{0.90}Mn_{0.10}O_2$, respectively. These starting materials were prepared using the coprecipitation method as previously described.[11,21] The electrochemical deintercalation was carried out in Li/liquid electrolyte/positive electrode lithium batteries. The positive electrodes consisted of a mixture of 90 wt % of active material and 10% of carbon black/graphite (1:1); no binder was used, but the positive electrode mixture was pressed in order to have a good electronic contact between the grains and, therefore, to prevent cell polarization. $LiPF_6$ (1 M) dissolved in a mixture of propylene carbonate (PC), ethylene carbonate (EC), and dimethyl carbonate (DMC) (1:1:3 by volume) was used as electrolyte. The cells were assembled and charged at room temperature in an argon-filled drybox; a slow cycling rate (C/200, with C corresponding to a theoretical exchange of one electron in 1 h during charge) was used in galvanostatic mode, with alternative periods of relaxation in order to be close to the thermodynamic equilibrium. When charged to the desired lithium compositions, the positive electrodes were removed from the cells, washed with DMC, and then dried under vacuum.

Thermal gravimetric analyses coupled with mass spectrometry were carried out under an argon stream, from room temperature to 600 °C, with a heating rate of 5 °C/min. Samples of about 30 mg were used. The X-ray diffraction patterns of the end products were recorded in the 10−80° (2θ) range (0.02°/1 s) using a Siemens D5000 powder diffractometer with Cu Kα radiation and a graphite diffracted beam monochromator. As only a small amount of powder was available, it was not possible to completely cover the surface of the polycarbonate diffraction sample-holder. Therefore, the corresponding XRD patterns are characterized by a high-level background.

X-ray diffraction patterns were recorded in situ upon increasing temperature, by using a capillary furnace on an Inel CPS 120 diffractometer with Co $K\alpha_1$ radiation; for convenience, all the data will be referred in the following to the Cu $K\alpha_1$ radiation. The $Li_xNi_{0.70}Co_{0.15}Al_{0.15}O_2$ and $Li_xNi_{0.90}Mn_{0.10}O_2$ deintercalated phases were introduced in 0.50-mm diam capillaries that were sealed and then heated by stage from room temperature to 300 °C, with a heating rate of 15 °C/min. At each step, an XRD pattern was recorded during 1 h, after a stabilization of the temperature during 10 min.

Results

$Li_xNi_{0.70}Co_{0.15}Al_{0.15}O_2$ Phases. Figure 1 shows the TGA/MS experiments from the $Li_{0.50}Ni_{0.70}Co_{0.15}Al_{0.15}O_2$ and $Li_{0.30}Ni_{0.70}Co_{0.15}Al_{0.15}O_2$ phases. As already observed for $Li_xNi_{1.02}O_2$ and $Li_xNi_{0.89}Al_{0.16}O_2$, weight losses occurring upon thermal treatment correspond mainly to oxygen releases.[1] Note that release of water and desorption of CO_2 were shown to be very small; it was, therefore, not possible to take them into account. For $Li_{0.50}Ni_{0.70}Co_{0.15}Al_{0.15}O_2$, a single oxygen release peak is observed, starting around 295 °C. For $Li_{0.30}Ni_{0.70}Co_{0.15}Al_{0.15}O_2$, a similar thermal behavior is observed, but with an additional oxygen release occurring at lower temperature (near 215 °C); these two contributions correspond likely to the two steps of the degradation process described in the Part I of this paper.[1]

The XRD patterns recorded at the end of the TGA/MS experiments show, as observed in Figure 2 in the particular case of $Li_{0.30}Ni_{0.70}Co_{0.15}Al_{0.15}O_2$, that the materials are characterized by a NiO-type structure (space group $Fm3m$) after being heated to 600 °C. The theoretical weight losses, corresponding to the structural transition 1 or 2 between the initial phase and the NiO-type phases, are in good agreement with the experimental values: $(\Delta m)_{th.} = 8.94\%$ vs $(\Delta m)_{exp.} = 8.9\%$ for $Li_{0.50}Ni_{0.70}Co_{0.15}Al_{0.15}O_2$ and $(\Delta m)_{th.} = 12.72\%$ vs $(\Delta m)_{exp.} = 12.6\%$ for $Li_{0.30}Ni_{0.70}Co_{0.15}Al_{0.15}O_2$.

$$Li_{0.50}Ni_{0.70}Co_{0.15}Al_{0.15}O_2 \rightarrow 1.5\,(Li_{0.33}Ni_{0.47}Co_{0.10}Al_{0.10}O) + 0.25\,O_2 \quad (1)$$

$$Li_{0.30}Ni_{0.70}Co_{0.15}Al_{0.15}O_2 \rightarrow 1.3\,(Li_{0.23}Ni_{0.54}Co_{0.12}Al_{0.12}O) + 0.35\,O_2 \quad (2)$$

Figure 3 shows the XRD patterns recorded in situ for $Li_{0.50}Ni_{0.70}Co_{0.15}Al_{0.15}O_2$ and $Li_{0.30}Ni_{0.70}Co_{0.15}Al_{0.15}O_2$ upon

(10) Ohzuku, T.; Yanagawa, T.; Kouguchi, M.; Ueda, A. *J. Power Sources* **1997**, *68*, 131.
(11) Guilmard, M.; Pouillerie, C.; Croguennec, L.; Delmas, C. *Solid State Ionics* **2003**, *60*, 39.
(12) Biensan, P.; Pérès, J. P.; Perton, F. The 1999 Joint International Meeting of the Electrochemical Society, Hawaii, October 17−22, 1999.
(13) Madhavi, S.; Subba Rao, G. V.; Chowdari, B. V. R.; Li, S. F. Y. *J. Power Sources* **2001**, *93*, 156.
(14) Lee, K. K.; Yoon, W. S.; Kim, K. B.; Lee, K. Y.; Hong, S. T. *J. Power Sources* **2001**, *97−98*, 308.
(15) Weaving, J. S.; Coowar, F.; Teagle, D. A.; Cullen, J.; Dass, V.; Bindin, P.; Green, R.; Macklin, W. J. *J. Power Sources* **2001**, *97−98*, 733.
(16) Arai, H.; Okada, S.; Sakurai, Y.; Yamaki, J. *J. Electrochem. Soc.* **1997**, *144*, 3117.
(17) Novak, P.; Nesper, R.; Coluccia, M.; Joho, F.; Piotto Piotto, A. *Extended Abstract of the Lithium Battery Discussion: Electrode Materials*; Arcachon, France, May 27 − June 1, 2001, abstract 56.
(18) MacNeil, D. D.; Lu, Z.; Chen, Z.; Dahn, J. R. *J. Power Sources* **2002**, *108*, 8.
(19) Ohzuku, T.; Makimura, Y. *Chem. Lett.* **2001**, 744.
(20) Makimura, Y.; Terada, N.; Ohzuku, T. *The 43rd Battery Symposium in Japan*; Fukuoka (Japan), October, 12−14, 2002; page 36.
(21) Guilmard, M.; Croguennec, L.; Delmas, C. *J. Electrochem. Soc.* in press.

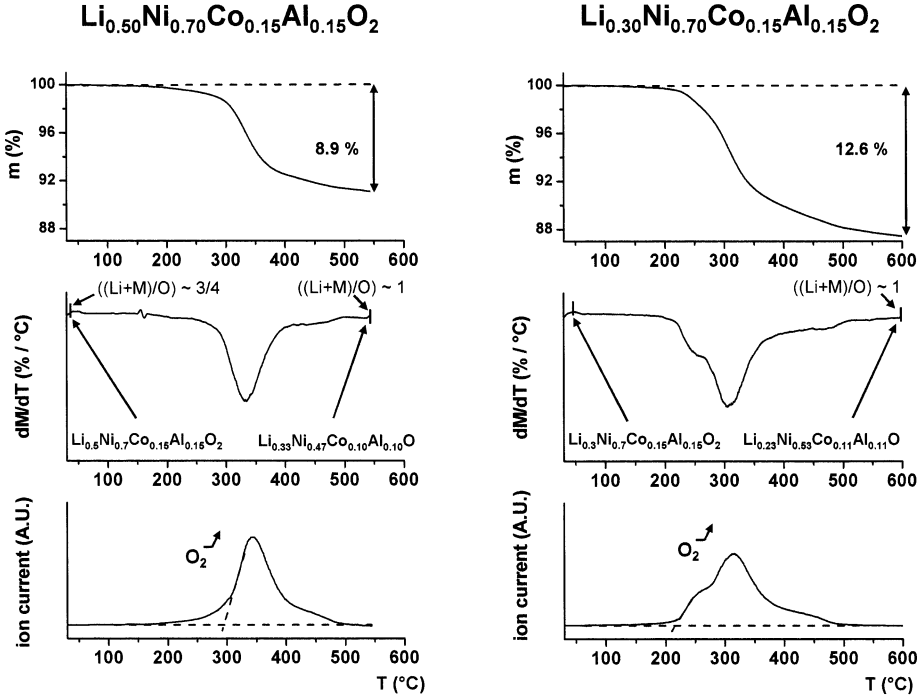

Figure 1. Thermal gravimetric analyses coupled with mass spectrometry for $Li_{0.50}Ni_{0.70}Co_{0.15}Al_{0.15}O_2$ and $Li_{0.30}Ni_{0.70}Co_{0.15}Al_{0.15}O_2$ (sample mass ~30 mg, heating rate of 5 °C/min under an argon stream). The ((Li + M)/O) ratios and chemical compositions are given before and after each oxygen release.

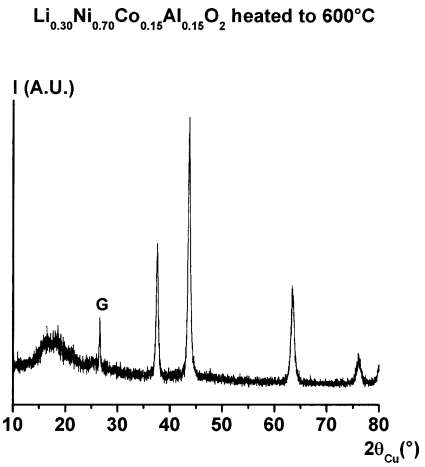

Figure 2. X-ray diffraction pattern recorded for $Li_{0.30}Ni_{0.70}Co_{0.15}Al_{0.15}O_2$ after the TGA/MS experiment (performed up to 600 °C).

increasing temperature, between room temperature and 300 °C. As already observed for the $Li_xNi_{1.02}O_2$ and $Li_xNi_{0.89}Al_{0.16}O_2$ compounds, there is a first structural transition between the lamellar α-$NaFeO_2$-type phase ($R\bar{3}m$) and a cubic "LiM_2O_4" pseudo-spinel-type phase ($Fd3m$). Indeed, above 170/180 °C, the (018)/(110) diffraction lines of the $R\bar{3}m$ space group merge progressively into the (440) single line of the $Fd3m$ space group, and the intensity of the (220) diffraction line, characteristic of the $Fd3m$ space group, increases. Nevertheless, the analysis of these XRD patterns appears to be more complex than that for $Li_xNi_{1.02}O_2$ and $Li_xNi_{0.89}Al_{0.16}O_2$, with the presence of several phases evolving in parallel but with different transition temperatures. This result is in agreement with the conclusions drawn from the Rietveld refinement of the neutron diffraction data, which has shown for $LiNi_{0.70}Co_{0.15}Al_{0.15}O_2$ a tendency for cobalt/aluminum segregation with the formation of several neighboring phases.[11] Note that the second transition between the pseudo-spinel phase and the NiO-type phase is not observed in this figure due to a limitation in temperature for the furnace (300 °C): indeed, the formation of the NiO-type structure is observed for the $Li_xNi_{0.70}Co_{0.15}Al_{0.15}O_2$ compounds, but over 300 °C, as shown by the XRD patterns recorded after the TGA/MS analyses (Figure 2).

To resume, the same type of degradation mechanism occurs for $Li_xNi_{0.70}Co_{0.15}Al_{0.15}O_2$ as for $Li_xNi_{0.89}Al_{0.16}O_2$ and Li_xNiO_2: indeed the structure evolves from a 2D structural type to a 3D NiO-type through two steps. The first transition clearly observed on the XRD patterns corresponds to the formation through a solid solution reaction of a LiM_2O_4 pseudo-spinel-type phase; the second transition observed by TGA/MS leads to the formation of a NiO-type phase.

$Li_xNi_{0.90}Mn_{0.10}O_2$ Phases. The thermal degradation mechanism of low-manganese-substituted materials appears to be the same as the one already determined for $Li_xNi_{1.02}O_2$, $Li_xNi_{0.89}Al_{0.16}O_2$, and $Li_xNi_{0.70}Co_{0.15}Al_{0.15}O_2$. Indeed, as observed in Figure 4, the TGA/MS measurements show weight losses upon increasing temperature that are mainly due to oxygen release. A single peak (near 315 °C) is observed on the weight loss derivative curve of $Li_{0.50}Ni_{0.90}Mn_{0.10}O_2$, whereas an additional peak corresponding to the first step (layered to spinel-type phase) of the degradation mechanism is observed at lower temperature (near 195 °C) for $Li_{0.30}Ni_{0.90}Mn_{0.10}O_2$. $Li_xNi_{0.90}Mn_{0.10}O_2$ materials recovered at the end of the TGA/MS experiment are also characterized by a NiO-type structure, as shown in Figure 5 in the particular case of $Li_{0.30}Ni_{0.90}Mn_{0.10}O_2$. Good agreement is observed between the experimental weight

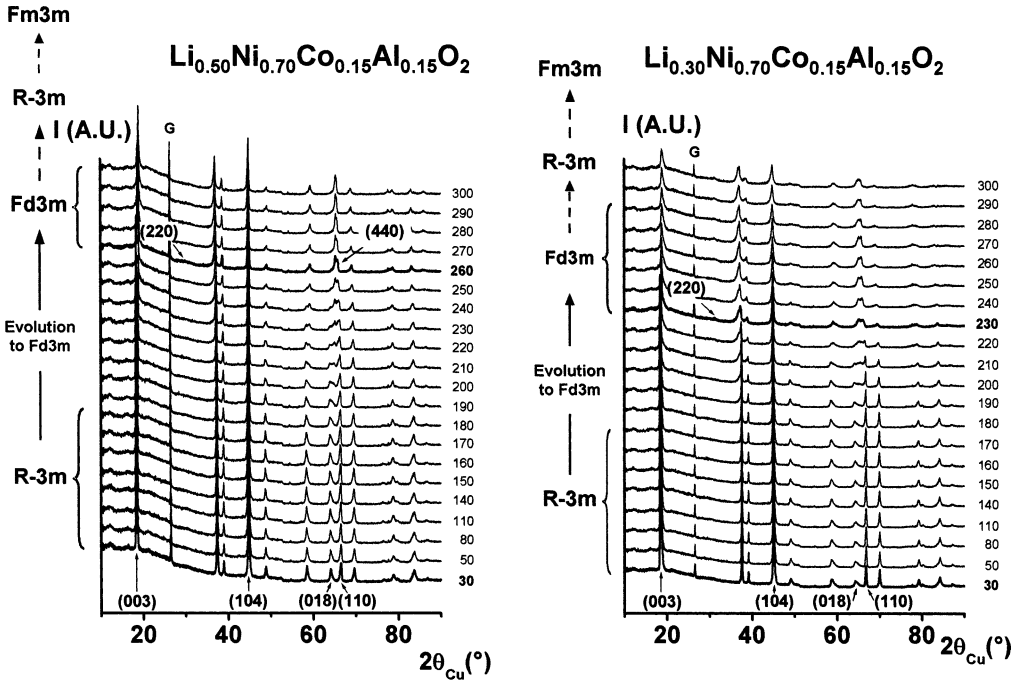

Figure 3. In situ X-ray diffraction patterns of $Li_{0.50}Ni_{0.70}Co_{0.15}Al_{0.15}O_2$ and $Li_{0.30}Ni_{0.70}Co_{0.15}Al_{0.15}O_2$ upon increasing temperature (heating rate 15 °C/min, waiting time before measurement at each temperature step 10 min, and acquisition time of 1 h).

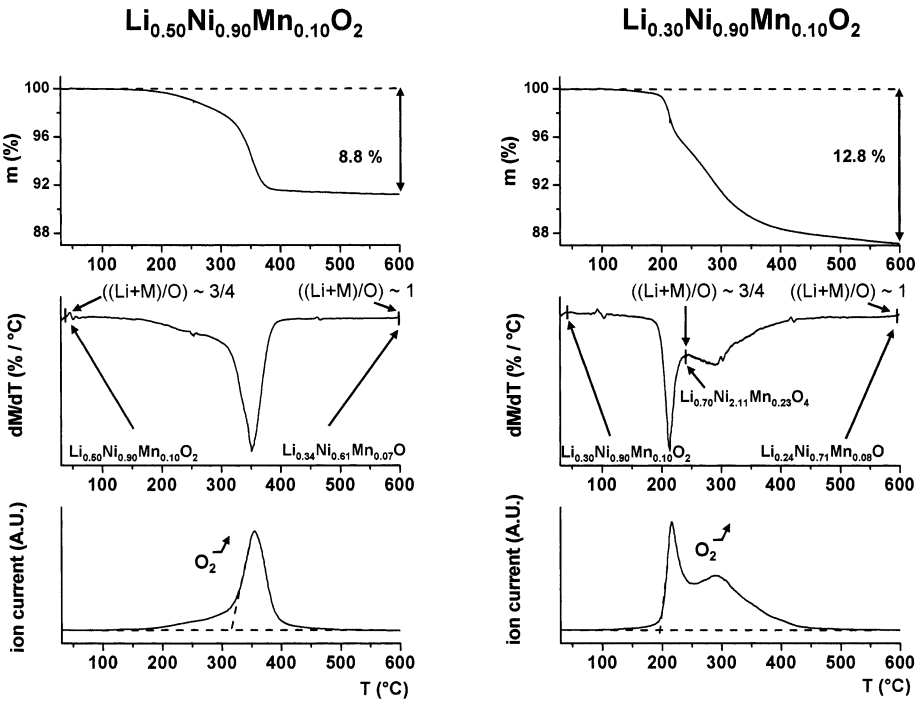

Figure 4. Thermal gravimetric analyses coupled with mass spectrometry for $Li_{0.50}Ni_{0.90}Mn_{0.10}O_2$ and $Li_{0.30}Ni_{0.90}Mn_{0.10}O_2$ (sample mass ~30 mg, heating rate of 5 °C/min under an argon stream). The ((Li + M)/O) ratios and chemical compositions are given before and after each oxygen release.

losses and the calculated ones, assuming the following reactions:

$$Li_{0.50}Ni_{0.90}Mn_{0.10}O_2 \rightarrow 1.5\,(Li_{0.33}Ni_{0.60}Mn_{0.07}O) + 0.25\,O_2 \quad (3)$$

$$((\Delta m)_{th.} = 8.53\ \%\ \text{vs.}\ (\Delta m)_{exp.} = 8.8\ \%)$$

$$Li_{0.30}Ni_{0.90}Mn_{0.10}O_2 \rightarrow 1.3\,(Li_{0.23}Ni_{0.69}Mn_{0.08}O) + 0.35\,O_2 \quad (4)$$

$$((\Delta m)_{th.} = 12.12\ \%\ \text{vs.}\ (\Delta m)_{exp.} = 12.8\ \%)$$

The XRD patterns recorded in situ for $Li_{0.50}Ni_{0.90}Mn_{0.10}O_2$ and $Li_{0.30}Ni_{0.90}Mn_{0.10}O_2$ upon increasing temperature are presented in Figure 6; they confirm the degradation mechanism assumed from the TGA/MS measurements. The two steps of the mechanism are clearly observed for $Li_{0.30}Ni_{0.90}Mn_{0.10}O_2$, with the apparition of the pseudo-spinel-type phase at 180 °C and of the highly disordered $R\bar{3}m$ type structure at 300 °C. Only the first step is observed for $Li_{0.50}Ni_{0.90}Mn_{0.10}O_2$, (apparition of the pseudo-spinel phase at 240 °C), the second one occurring at a temperature higher than 300 °C.

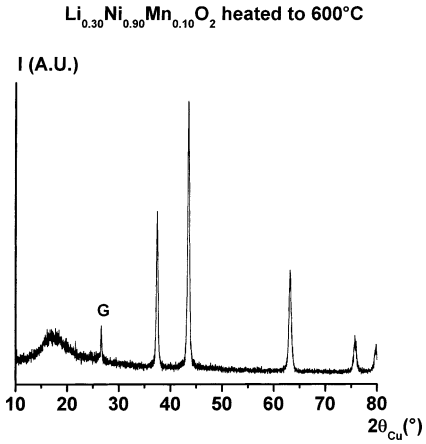

Figure 5. X-ray diffraction pattern recorded for $Li_{0.30}Ni_{0.90}Mn_{0.10}O_2$ after the TGA/MS experiment (performed up to 600 °C).

Comparison of the Thermal Stability of the $Li_xNi_{1.02}O_2$, $Li_xNi_{0.89}Al_{0.16}O_2$, $Li_xNi_{0.70}Co_{0.15}Al_{0.15}O_2$, and $Li_xNi_{0.90}Mn_{0.10}O_2$ Materials. In this section we report a general comparison of the behavior of the four materials. For this purpose, experimental results described in this paper are discussed together with those presented in the companion paper (Part I).

A similar degradation mechanism is observed for the four materials ($Li_xNi_{1.02}O_2$, $Li_xNi_{0.89}Al_{0.16}O_2$, $Li_xNi_{0.70}Co_{0.15}Al_{0.15}O_2$, and $Li_xNi_{0.90}Mn_{0.10}O_2$). It occurs in two steps. The first step, corresponding to the structural transition between the initial lamellar α-$NaFeO_2$-type phase and a LiM_2O_4 pseudo-spinel-type phase, is associated with an oxygen release only for a lithium content smaller than 0.50. The second step corresponds to the transition between the LiM_2O_4 pseudo-spinel-type phase and a NiO-type phase, through the formation of a highly disordered $R\bar{3}m$ phase. This second step is associated with an oxygen release, regardless of the lithium content.

In the following, the results obtained from the $Li_{0.50}MO_2$ and $Li_{0.30}MO_2$ compositions will be compared successively.

Table 1. Comparison for $Li_{0.50}Ni_{1.02}O_2$, $Li_{0.50}Ni_{0.89}Al_{0.16}O_2$, $Li_{0.50}Ni_{0.70}Co_{0.15}Al_{0.15}O_2$, and $Li_{0.50}Ni_{0.90}Mn_{0.10}O_2$ of the Pseudo-Spinel Formation Temperatures Determined According to the in situ XRD Experiments, and of the Oxygen Release Onset Temperatures Determined According to the TGA/MS Experiments

	first step: *T* (°C) of the pseudo-spinel phase formation (XRD)	second step: O_2 release onset *T* (°C) (TGA/MS)
$Li_{0.50}Ni_{1.02}O_2$[a]	200	265
$Li_{0.50}Ni_{0.89}Al_{0.16}O_2$[a]	240	290
$Li_{0.50}Ni_{0.70}Co_{0.15}Al_{0.15}O_2$	260	295
$Li_{0.50}Ni_{0.90}Mn_{0.10}O_2$	240	315

[a] Part I, Ref 1.

$Li_{0.50}MO_2$ Phases: First Step. From the previously described experiments, for a lithium content equal to 0.50, the first step of the mechanism can be observed only by the in situ XRD experiments because no oxygen release occurs during the pseudo-spinel formation due to a (Li + M)/O initial ratio equal to $^3/_4$. Table 1 presents the temperature of the pseudo-spinel-type phase formation determined according to the XRD patterns for the four types of studied materials. As shown in this table, the pseudo-spinel-type phase is formed at the highest temperature for $Li_{0.50}Ni_{0.70}Co_{0.15}Al_{0.15}O_2$ (T = 260 °C). Partial aluminum or manganese substitution also has a positive effect on the thermal stability of the initial lamellar phase, as the pseudo-spinel phase is formed in both cases at a higher temperature than that for $Li_{0.50}NiO_2$ (240 °C vs 200 °C, respectively). The materials concerned in this study crystallize either in the monoclinic ($C2/m$), in the hexagonal ($R\bar{3}m$) or in the cubic ($Fd3m$) systems; therefore, to allow a general comparison, in each case the hypothetical $a_{hex.}$ and $c_{hex.}$ parameters were deduced from the real cells. The cell parameter determination was not obvious in the $Li_xNi_{0.70}Co_{0.15}Al_{0.15}O_2$ case, as several phases closely related are obtained. The evolution of the $c_{hex.}/a_{hex.}$ ratio vs temperature is presented in Figure 7 (a) for $Li_{0.50}MO_2$ compounds; it illustrates well the stabilizing effect of

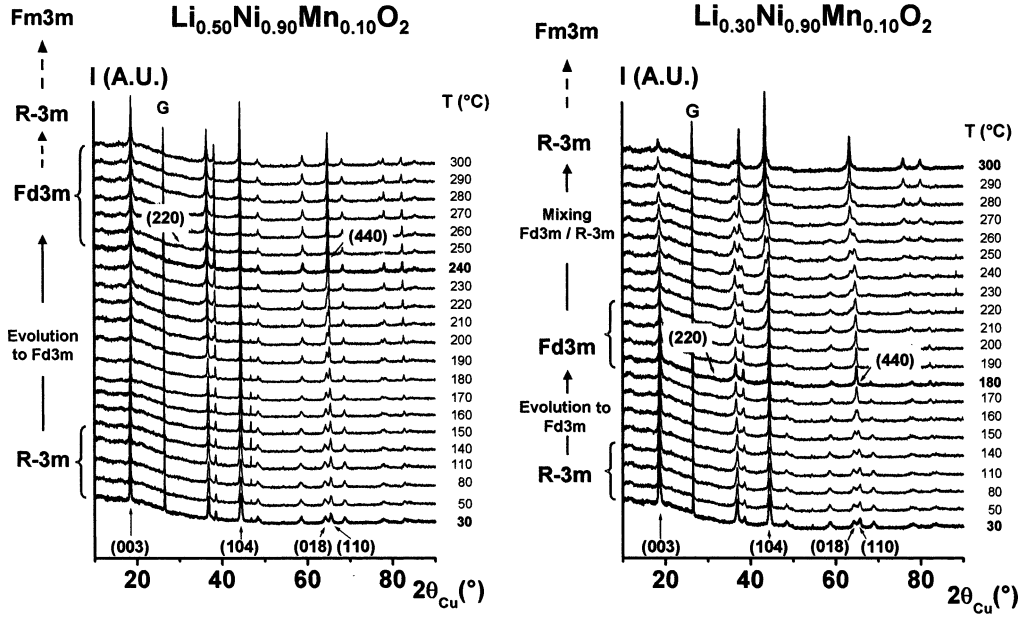

Figure 6. In situ X-ray diffraction patterns of $Li_{0.50}Ni_{0.90}Mn_{0.10}O_2$ and $Li_{0.30}Ni_{0.90}Mn_{0.10}O_2$ upon increasing temperature (heating rate 15 °C/min, waiting time before measurement at each temperature step 10 min, and acquisition time of 1 h).

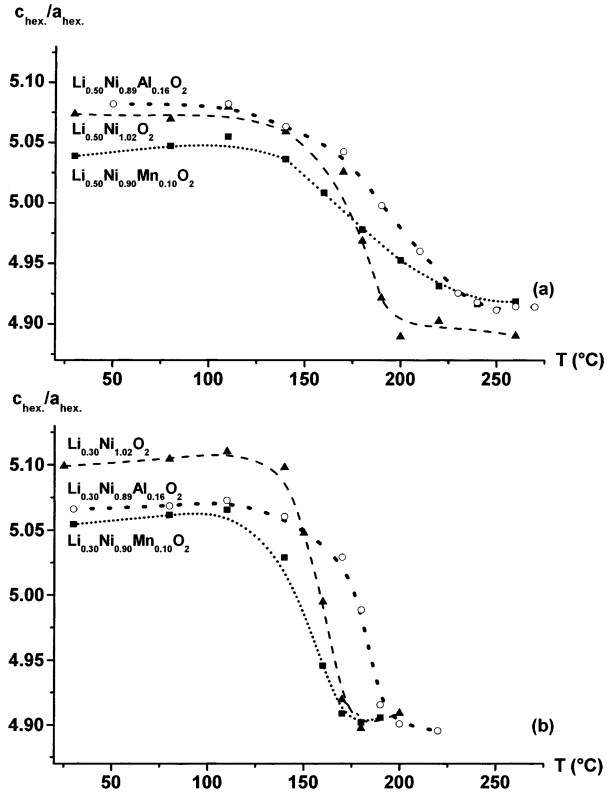

Figure 7. Evolution of the $c_{hex.}/a_{hex.}$ ratio versus temperature for $Li_xNi_{1.02}O_2$ (−▲−), $Li_xNi_{0.89}Al_{0.16}O_2$ (-○-), and $Li_xNi_{0.90}Mn_{0.10}O_2$ (·■·) (x = 0.50 (a) and 0.30 (b)). The $a_{hex.}$ and $c_{hex.}$ parameters were calculated from the X-ray diffraction patterns recorded in situ upon increasing temperature.

partial aluminum or manganese substitution. Indeed, the decrease of the $c_{hex.}/a_{hex.}$ ratio is slow, and the 4.90 final value, corresponding to the theoretical value for a cubic structure, is reached at a higher temperature for the substituted materials.

$Li_{0.50}MO_2$ Phases: Second Step. The second step can be followed only by TGA/MS measurements, as the upper temperature of the furnace used for the in situ XRD experiment is limited to 300 °C. A comparison of the oxygen release of the four materials is presented in Figure 8 (a). To compare the various materials, we chose the temperature corresponding to the extrapolation of the oxygen release peak as a reference. Indeed, the oxygen losses observed at lower temperature are overevaluated due to the water loss. Moreover, these low losses do not correspond to the major evolution of the material. As observed in this figure, the oxygen release onset temperature is the highest for $Li_{0.50}Ni_{0.90}Mn_{0.10}O_2$. Indeed, it occurs at 315 °C vs 295 °C for $Li_{0.50}Ni_{0.70}Co_{0.15}Al_{0.15}O_2$, 290 °C for $Li_{0.50}Ni_{0.89}Al_{0.16}O_2$, and 265 °C for $Li_{0.50}Ni_{1.02}O_2$ (Table 1). The partial manganese substitution appears therefore very efficient to stabilize the pseudo-spinel phase for a lithium content equal to 0.50.

$Li_{0.30}MO_2$ Phases: First Step. For a lithium content equal to 0.30, the first step of the mechanism can be observed either by in situ XRD or TGA/MS experiments, as the formation of the pseudo-spinel-type phase is associated with an oxygen release. Table 2 presents the temperature of the pseudo-spinel formation deduced from the in situ XRD patterns and from the oxygen release onset temperature corresponding to this transformation (Figure 8b). Note that the differences in temperature observed between the XRD and the TGA/MS experiments are due to kinetics. As expected and as previously shown by Dahn, the oxygen release onset temperature is very dependent on the heating rate.[22] Indeed, oxygen losses appear at lower temperatures for the XRD experiments because of a much slower heating rate (around 20 h is necessary to reach 300 °C) than the one used for the TGA/MS analyses (5 °C/min: only 55 min is necessary to reach 300 °C). As observed in Table 2, the pseudo-spinel-type phase is formed at the highest temperature for $Li_{0.30}Ni_{0.70}Co_{0.15}Al_{0.15}O_2$ (T = 230 °C according to the in situ XRD patterns). An improvement of the stability of the initial phase is also observed for $Li_{0.30}Ni_{0.89}Al_{0.16}O_2$ (T = 200 °C) in com-

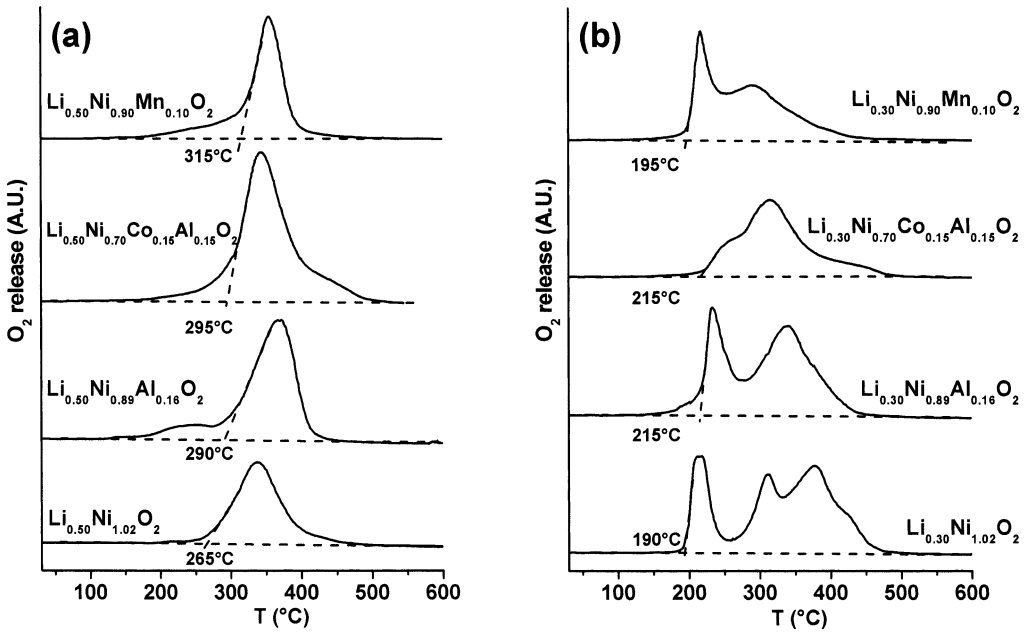

Figure 8. Comparison of the O_2 release versus temperature for $Li_xNi_{1.02}O_2$, $Li_xNi_{0.89}Al_{0.16}O_2$, $Li_xNi_{0.70}Co_{0.15}Al_{0.15}O_2$, and $Li_xNi_{0.90}Mn_{0.10}O_2$ (x = 0.50 (a) and 0.30 (b)) (sample mass ∼30 mg, heating rate of 5 °C/min under an argon stream). The data have been offset vertically for clarity.

Table 2. Comparison for $Li_{0.30}Ni_{1.02}O_2$, $Li_{0.30}Ni_{0.89}Al_{0.16}O_2$, $Li_{0.30}Ni_{0.70}Co_{0.15}Al_{0.15}O_2$, and $Li_{0.30}Ni_{0.90}Mn_{0.10}O_2$ of the Pseudo-Spinel and Disordered $R\bar{3}m$ Phase Formation Temperatures, Determined According to the in Situ XRD Experiments, and of the Oxygen Release Onset Temperatures, Determined According to the TGA/MS Experiments

	first step		second step
	T (°C) of the pseudo-spinel phase formation (XRD)	O_2 release onset T (°C) first peak (TGA/MS)	T (°C) of the disordered $R\bar{3}m$ phase formation (XRD)
$Li_{0.30}Ni_{1.02}O_2$ (Part I)	180	190	270
$Li_{0.30}Ni_{0.89}Al_{0.16}O_2$ (Part I)	200	215	>300
$Li_{0.30}Ni_{0.70}Co_{0.15}Al_{0.15}O_2$	230	215	>300
$Li_{0.30}Ni_{0.90}Mn_{0.10}O_2$	180	195	300

parison with $Li_{0.30}Ni_{1.02}O_2$ ($T = 180$ °C). On the contrary, no improvement is observed for $Li_{0.30}Ni_{0.90}Mn_{0.10}O_2$ during the first step of the degradation mechanism. The evolution of the $c_{hex.}/a_{hex.}$ ratio vs temperature for $Li_{0.30}Ni_{1.02}O_2$, $Li_{0.30}Ni_{0.89}Al_{0.16}O_2$ and $Li_{0.30}Ni_{0.90}Mn_{0.10}O_2$ presented in Figure 7b illustrates well the stabilizing effect of partial aluminum substitution and the absence of any stabilization with the partial manganese substitution.

Note that the layered to spinel transition occurs in a narrower temperature range for $Li_{0.30}MO_2$ phases than for the $Li_{0.50}MO_2$ phases, even in the case of the $Li_xNi_{0.89}Al_{0.16}O_2$ system which is stabilized. This difference in behavior can result from the difference in reaction mechanisms: for the $Li_{0.50}MO_2$ compositions only a cationic migration is required, while for the $Li_{0.30}MO_2$ ones, a structural reorganization of the material occurs as oxygen is removed.

$Li_{0.30}MO_2$ Phases: Second Step. The second step of the thermal degradation mechanism corresponds to the second peak due to oxygen release observed in the TGA/MS experiments. This second step can also be observed partially for $Li_{0.30}Ni_{1.02}O_2$ (Figure 7 in the companion paper (Part I))[1] and $Li_{0.30}Ni_{0.90}Mn_{0.10}O_2$ (Figure 6) on the in situ XRD patterns. Indeed, the complete evolution to the highly disordered $R\bar{3}m$ phase is observed for these two compounds. The pseudo-spinel-type phase disappears at a higher temperature for $Li_{0.30}Ni_{0.90}Mn_{0.10}O_2$ ($T = 300$ °C) than for $Li_{0.30}Ni_{1.02}O_2$ ($T = 270$ °C), which confirms the stabilizing effect of the manganese partial substitution on the pseudo-spinel-type phase. For $Li_{0.30}Ni_{0.89}Al_{0.16}O_2$ and $Li_{0.30}Ni_{0.70}Co_{0.15}Al_{0.15}O_2$, the pseudo-spinel-type phase has not yet completely disappeared at 300 °C, showing thus that the two corresponding pseudo-spinel-type phases are more stable. As shown in Figure 8b by the TGA/MS experiments, the oxygen release corresponding to the second structural transition seems to occur at a higher temperature for $Li_{0.30}Ni_{0.89}Al_{0.16}O_2$ than for $Li_{0.30}Ni_{0.70}Co_{0.15}Al_{0.15}O_2$.

Discussion

The irreversible chemical and structural modifications occurring during the thermal treatment of the $Li_x(Ni,M)O_2$ phases are very similar regardless of the composition of the starting material. In all cases, a layered ⇒ pseudo-spinel transition is observed in a first step followed by a pseudo-spinel ⇒ rocksalt transition at higher temperature. Although an oxygen evolution is observed in all cases during the second transition, it occurs only for $x < 0.5$ during the first transition. The main differences in thermal behavior between these various materials are: (i) the transition temperatures, (ii) the reaction energy, and (iii) the reaction kinetics. All these points are essential from an application point of view: a small change in the temperature (i.e., 30 to 50 degrees) required to initiate the first phase transition can modify to a very large extent the behavior of a practical cell.

Therefore, it is interesting to try to understand, from a general point of view, the thermal behavior of the materials considered in this study. The following points have to be considered.

(a) The stability of the structure which is related to the difference between the experimental composition and the ideal one (i.e., $LiMO_2$ for the layered phases and LiM_2O_4 for the spinel ones). Moreover, for a layered material, the intrinsic stability depends also on the ionicity of the M−O bonds (i.e., in oxides, on the electronegativity of the M element).

(b) The stability of the cation oxidation states in relation with their environment: indeed, Ni^{4+} and Co^{4+} ions are very unstable regardless of their coordination polyhedron; Ni^{3+} and Mn^{3+} ions are unstable only in a tetrahedral surrounding; and Al^{3+} ions are stable in both octahedral and tetrahedral environments. In all the structures considered in this study, the octahedra share edges; therefore, the size of each polyhedron does not depend only on the size of the cation, but also on the size of all the neighboring polyhedra. It follows that the modification of the crystal field by the neighboring cations affects the stability of a given oxidation state for a cation, and, as a result, that of the whole material.

(c) The ability for a given cation to move from an octahedral site to another one. This migration depends first on the stability of the involved cation in the intermediate tetrahedral site situated between two octahedra: Co^{3+}, Ni^{4+}, and Mn^{4+} ions are very unstable in tetrahedral sites, whereas Al^{3+} ions are very stable; Ni^{3+} can occupy a tetrahedral site after a low spin to high spin configuration modification, but this environment is not favorable.[23] The activation energy of the cationic transfer depends also on the interatomic distances in the polyhedron involved. Indeed, a Ni^{3+} ion in a lattice built mainly of small cations (Co^{3+}, Ni^{4+}, and Mn^{4+}) will move less easily to the interslab space than in a surrounding where the Ni^{3+} ions are prevailing: the presence of small cations leads to a bottleneck contraction.

The two first points concern the thermodynamical properties, whereas the last one is related to the kinetic properties; nevertheless, kinetics plays a very important

(22) Dahn, J. R.; Fuller, E. W.; Obrovac, M.; Von Sacken, U. *Solid State Ionics* **1994**, *69*, 265.

(23) Thomas, M. G. S. R.; David, W. I. F.; Goodenough, J. B.; Groves, P. *Mater. Res. Bull.* **1985**, *20*, 1137.

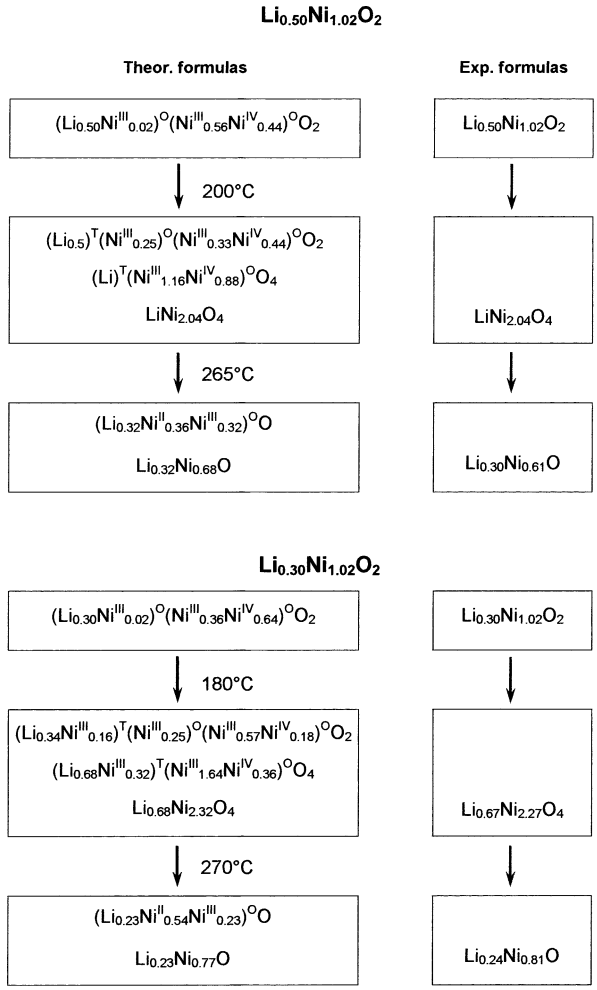

Figure 9. Theoretical changes in chemical compositions and formulas expected during the thermal treatment of $Li_{0.50}Ni_{1.02}O_2$ and $Li_{0.30}Ni_{1.02}O_2$ phases; the experimental values deduced from the TGA analyses are given on the right of the figure for comparison.

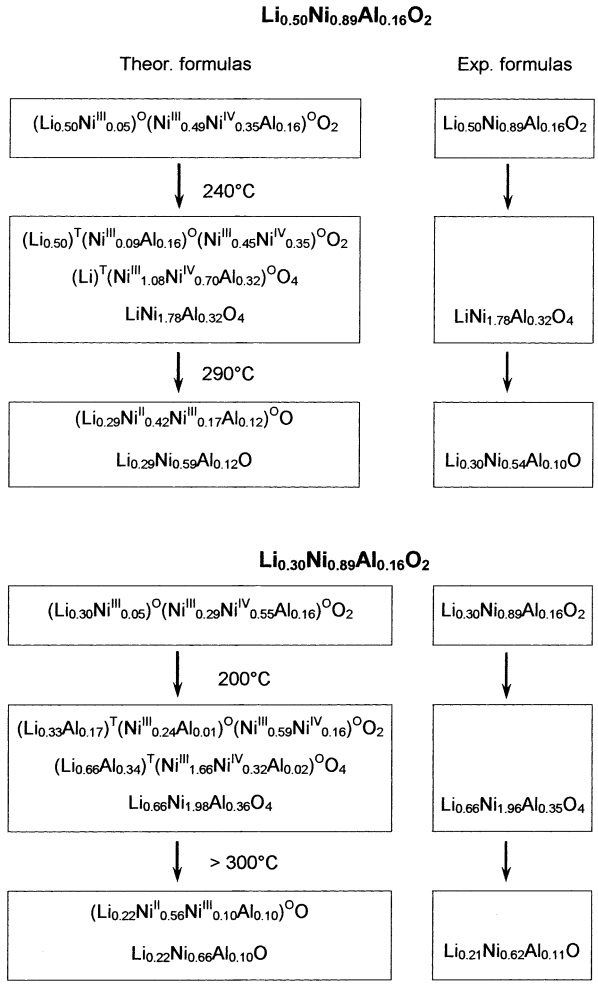

Figure 10. Theoretical changes in chemical compositions and formulas expected during the thermal treatment of $Li_{0.50}Ni_{0.89}Al_{0.16}O_2$ and $Li_{0.30}Ni_{0.89}Al_{0.16}O_2$ phases; the experimental values deduced from the TGA analyses are given on the right of the figure for comparison.

role: indeed, as the temperatures involved in these reactions are quite low (180−300 °C), the material metastability can delay the decomposition reaction.

From these general points, it is interesting to compare the effects of aluminum, cobalt, and manganese on the stability of deintercalated lithium nickelate. The two transitions that occur upon increasing temperature will be considered successively. In Figures 9 through 12, we have summarized for these different systems the theoretical changes in chemical compositions and formulas expected during the transitions; and the chemical compositions were compared to the experimental values deduced from the TGA. The theoretical formulas were proposed assuming the following hypotheses. (a) Upon oxidation, the oxidation states appear in the following order: Ni^{2+}, Co^{3+}, Mn^{4+}, Ni^{3+}, Ni^{4+}, and Co^{4+}. (b) In the spinel phase obtained after the first step, the tetrahedral sites are fully occupied and the oxygen lattice is considered as ideal. Two crystallographic formulas are given. The first one, $(Li_{0.5})^T(M_{0.25})^O(M_{0.75})^OO_2$, for example, corresponds to a layered description of a spinel and allows emphasis of the cationic migrations involved during the transition, whereas the second formula, $(Li)^T(M_2)^OO_4$, is the classical spinel one (the T and O exponents refer to tetrahedral and octahedral environments, respectively). (c) The formulas of the rocksalt phases obtained after the second step are considered as ideal [(Li,M)O].

As shown in Figures 9−12, the experimental formulas are in all cases in quite good agreement with the theoretical ones. For the spinel materials, the cationic excess observed after the first thermal treatment results from the departure from the ideal stoichiometry for the starting materials. In the case of the materials with the rocksalt structure, recovered at the end of the TGA experiments, very good agreement is observed between the experimental and the expected formulas. In some cases, a cationic deficiency is observed. This behavior results from the relatively low final temperature that allows the formation of rocksalt structure with cations in an oxidation state higher than 2.

The Layered ⇒ Pseudo-Spinel Transition. This transition depends on the instability of the layered structure; it occurs when a too large amount of lithium ions is deintercalated. This effect is clearly shown by the lower transition temperature observed for the $Li_{0.30}$ phases than for the $Li_{0.50}$ phases. When the layered phase becomes no longer stable, some ions move from the slab to the interslab space; their amount increases, until reaching an overall distribution of trivalent and tetravalent cations close to the spinel one. At this step, the oxygen packing is very close to the ideal *cfc* lattice

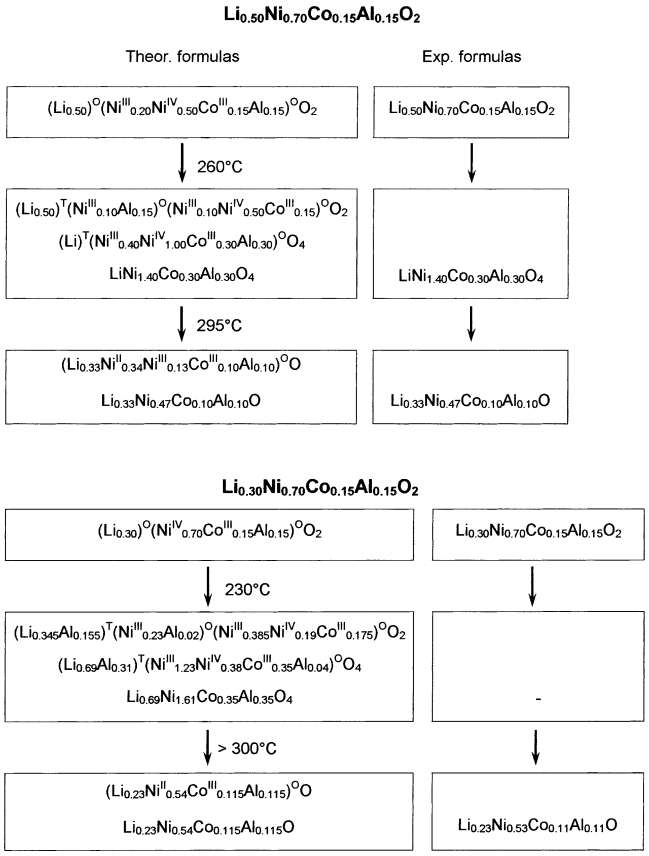

Figure 11. Theoretical changes in chemical compositions and formulas expected during the thermal treatment of $Li_{0.50}Ni_{0.70}Co_{0.15}Al_{0.15}O_2$ and $Li_{0.30}Ni_{0.70}Co_{0.15}Al_{0.15}O_2$ phases; the experimental values deduced from the TGA analyses are given on the right of the figure for comparison. It was not possible to separate the 1st oxygen loss from the 2nd one and, therefore, to deduce from TGA analyses the composition of the spinel phase formed for $Li_{0.30}Ni_{0.70}Co_{0.15}Al_{0.15}O_2$.

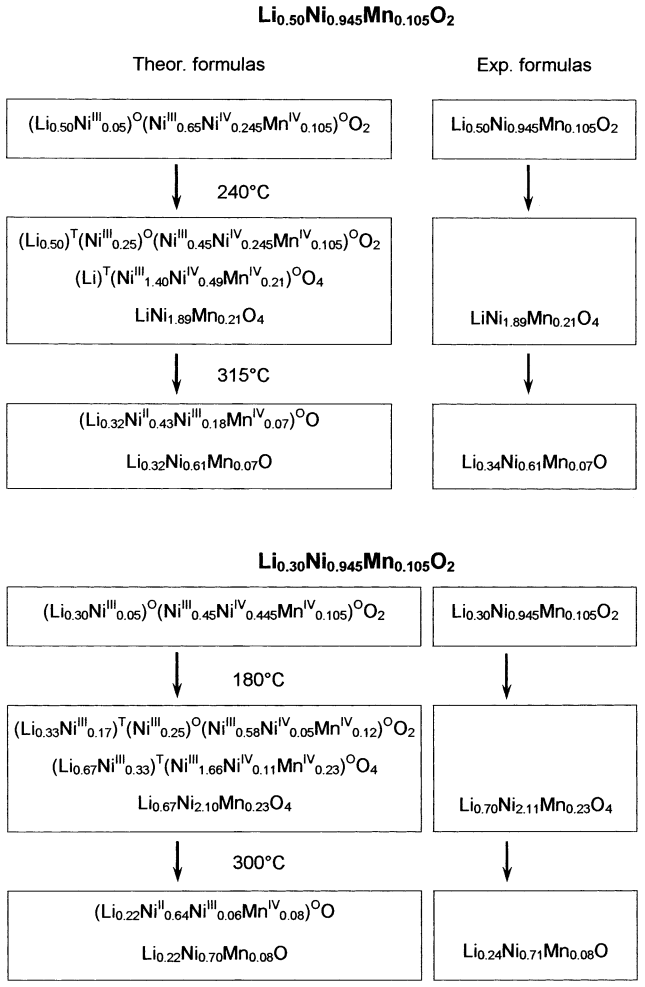

Figure 12. Theoretical changes in chemical compositions and formulas expected during the thermal treatment of $Li_{0.50}Ni_{0.945}Mn_{0.105}O_2$ and $Li_{0.30}Ni_{0.945}Mn_{0.105}O_2$ phases; the experimental values deduced from the TGA analyses are given on the right of the figure for comparison.

(Figure 12 in Part I[1]) and the octahedral sites of the interslab space become too small to accommodate the lithium ions that consequently move in the tetrahedral sites, leading to a pseudo-spinel type phase.

The cationic migration is very easy for Al^{3+} ions that are stable in both octahedral and tetrahedral sites, very difficult for Co^{3+}, Ni^{4+}, and Mn^{4+} ions, and difficult for Ni^{3+} ions, as previously discussed.

One can assume that in the case of the aluminum-substituted phases, the Al^{3+} ions move preferentially to the tetrahedral sites where they are stabilized, leading thus to the formation of intermediate cationic distributions which explain the small slope of the $c_{hex.}/a_{hex.} = f(T)$ curve (Figure 7). In the case of the aluminum-substituted phases, the formation of the pseudo-spinel phase is, therefore, observed at a higher temperature than it is in the pure nickel phase. One must also consider that in these aluminum-substituted phases the lattice contraction due to the presence of a large amount of small cations such as Ni^{4+} and Al^{3+} (and also Co^{3+} for $Li_{0.50}Ni_{0.70}Co_{0.15}Al_{0.15}O_2$) tends to increase the activation energy necessary for the cationic migration to occur, and, therefore, to delay the layered ⇒ pseudo-spinel transition.

In the case of the manganese-substituted phases, the temperature of the layered ⇒ pseudo-spinel transition and the shape of the $c_{hex.}/a_{hex.} = f(T)$ curve (Figure 7) are very similar to thoses observed for the aluminum-substituted phases. This suggests thus the occurrence of similar processes at the microscopic scale in the two aluminum and manganese-substituted systems. Keeping in mind that (i) electronic exchange between Ni^{3+} and Mn^{4+} can lead to Ni^{4+} and Mn^{3+}, and that (ii) two Jahn−Teller Mn^{3+} ions can disproportionate into Mn^{2+} and Mn^{4+}, the intermediate formation of Mn^{2+} cannot be excluded.[24] This ion can move easily in tetrahedral site as it is observed when the Li_xMnO_2 phase is transformed into spinel upon lithium deintercalation.[25−27] It is, therefore, possible to explain the similar behavior of aluminum- and manganese-substituted phases upon thermal treatment of the $Li_{0.50}$ phases. Note that these cationic distributions with manganese in tetrahedral site were not reported in Figure 12.

Whereas in the case of the $Li_{0.50}$ phases the transition can be considered as pseudomorphic because the oxygen lattice is preserved, in the case of the $Li_{0.30}$ phases a

(24) Reed, J.; Ceder, G.; Van Der Ven, A. *Electrochem. Solid-State Lett.* **2001**, *4*, A78.
(25) Capitaine, F. Thesis. Bordeaux I, France, 1997.
(26) Armstrong, A. R.; Robertson, A. D.; Bruce, P. G. *Electrochim. Acta* **1999**, *45*, 285.
(27) Croguennec, L.; Deniard, P.; Brec, R. *J. Electrochem. Soc.* **1997**, *144*, 3323.

reconstruction reaction must occur since a significant amount of oxygen is lost. In this case, the thermal instability of the Ni^{4+} ions must play an important role on the reaction as it superimposes on the instability of the strongly deintercalated layered structures. The highest transition temperature (230 °C) is observed for the $Li_{0.30}Ni_{0.70}Co_{0.15}Al_{0.15}O_2$ phase that does not contain Ni^{3+} ions anymore, but only small amounts of Co^{3+} and Al^{3+} ions which tend to stabilize the Ni^{4+} ions (Figure 11). On the opposite, the lower transition temperature is observed for the $Li_{0.30}Ni_{0.945}Mn_{0.105}O_2$ phase that contains the larger amount of the large Ni^{3+} ions (Figure 12): the decrease of the crystal field at the Ni^{4+} site decreases its stability.

The Pseudo-Spinel ⇒ Rocksalt Transition. The decomposition temperature related to this transition depends mainly on three points: (a) how far the material composition is from the ideal spinel one; (b) the amount of tetravalent Ni^{4+} ions; and (c) the stability of the tetravalent cations present in the material.

The two first points play in opposite directions. Indeed, the $Li_{0.50}MO_2$ phases have an almost ideal spinel composition but contain also a larger amount of Ni^{4+} in comparison to the $Li_{0.30}MO_2$ phaases. For the $Li_{0.50}MO_2$ materials, the temperature of the second transition increases when the amount of Ni^{4+} decreases, except in the case of $Li_{0.50}Ni_{0.70}Co_{0.15}Al_{0.15}O_2$ which is one of the more stable phase although it contains a large amount of Ni^{4+} ions. In this case, the presence of small Co^{3+} and Al^{3+} ions strongly stabilizes the Ni^{4+} ions and then increases the spinel decomposition temperature.

The last point concerns the decomposition of the spinel phases formed from the $Li_{0.30}MO_2$ phases. Because in the first step of the decomposition reaction ($Li_{0.30}$ layered ⇒ $Li_{0.30}$ spinel) a significant part of the oxygen is lost, the amount of Ni^{4+} ions is smaller than that in the $Li_{0.50}$ spinel phases. Therefore, the transition temperatures related to the second step are higher for the $Li_{0.30}$ materials than for the $Li_{0.50}$ materials.

Acknowledgment. We thank P. Dagault and D. Denux for thermal analyses, P. Biensan, C. Jordy, and J.P. Pérès for fruitful discussions, and Saft and Région Aquitaine for financial support.

CM030340U